Electrochimica Acta 282 (2018) 634–641

Contents lists available at ScienceDirect

Electrochimica Acta

journal homepage: www.elsevier.com/locate/electacta

Nano-structured $GeNb_{18}O_{47}$ as novel anode host with superior lithium storage performance

Fanmin Ran [a], Xing Cheng [a], Haoxiang Yu [a], Runtian Zheng [a], Tingting Liu [a], Xifei Li [b], Ning Ren [c], Miao Shui [a], Jie Shu [a, *]

[a] Faculty of Materials Science and Chemical Engineering, Ningbo University, No. 818 Fenghua Road, Jiangbei District, Ningbo 315211, People's Republic of China
[b] Institute of Advanced Electrochemical Energy, Xi'an University of Technology, Xi'an 710048, People's Republic of China
[c] Zhejiang Chiwee Chuangyuan Industry Co., Ltd., Changxing 313199, People's Republic of China

ARTICLE INFO

Article history:
Received 8 May 2018
Received in revised form
7 June 2018
Accepted 15 June 2018
Available online 18 June 2018

Keywords:
$GeNb_{18}O_{47}$
Nanowires
Electrospinning
Anode
Lithium storage material

ABSTRACT

Nanostructures always have an advantage in electrochemical research. In this work, the $GeNb_{18}O_{47}$ nanowires are synthesized by an easy electrospinning method for the first time. We study morphologies and electrochemical properties of as-obtained $GeNb_{18}O_{47}$ nanowires via the X-ray diffraction, charge/discharge curve, cyclic voltammetry, scanning electron microscopy and transmission electron microscopy. As expected, $GeNb_{18}O_{47}$ nanowires exhibit impressive charge capacity of 216.9 mAh g^{-1} at a current density of 100 mA g^{-1} and high-capacity retention of 93.6% after 200 cycles. Electrochemical analyses show that $GeNb_{18}O_{47}$ nanowires exhibit the lower redox polarization, smaller charge transfer resistance and higher Li^+ diffusion coefficient compared with sol-gel formed bulk sample. Therefore, the $GeNb_{18}O_{47}$ nanowire is a promising active electrode material for the lithium batteries.

1. Introduction

With the growing concern about environmental degradation and serious resources depletion [1–5], both academic and industrial communities have been concerned about the lithium-ion batteries (LIBs) that is the important power sources in electrical/hybrid cars and portable electronic equipment due to their lightweight, environmental friendliness, low-cost and safety [6–13]. In conventional LIBs, graphite is a widespread commercial host material used as the anode material because of its environmental benignity, non toxic harmless, and low-cost [14–16]. However, It is easy to form the thick solid-electrolyte interface (SEI) layers and lithium dendrites on the surface of electrode, because of the working voltage of low to 0.1 V (*vs.* Li^+/Li). It can lead to capacity loss and longer diffusion path of Li^+, which makes the poor electrochemical properties of LIBs in larger current density [17–21]. To address these issues, titanium-based materials such as $Li_4Ti_5O_{12}$ have been reported as an alternative of anode materials for its compatibility with the electrolyte, high structure thermodynamic stability. As compared to the graphite, it has high safety and excellent circulation stability because its high working voltage of ~1.57 V can avoid the formation of SEI layer/lithium dendrites [22–29]. Unfortunately, the specific capacity and electronic conductivity of $Li_4Ti_5O_{12}$ are low [30–33]. As a consequence, it is very urgent to explore new anode materials with much larger capacities for $Li_4Ti_5O_{12}$.

In recent years, niobium-based oxides have attracted much attention in the field of electrochemistry compared with insertion-type anodes because of their higher theoretical capacity. For instance, $TiNb_2O_7$ will provide a high theoretical capacity of 387.6 mAh g^{-1} because of its multiple redox couples of Nb^{4+}/Nb^{3+}, Nb^{5+}/Nb^{4+} and Ti^{4+}/Ti^{3+} than $Li_4Ti_5O_{12}$ [34–44]. And several possible candidates for anode materials, such as $Ti_2Nb_{10}O_{29}$ [42–44], $WNb_{12}O_{33}$ [36,45], VNb_9O_{25} [46], $ZrNb_{24}O_{62}$ [47], $Cr_{0.5}Nb_{24.5}O_{62}$ [48] and $FeNb_{11}O_{29}$ [49] have also been proposed and investigated. All of them display efficient lithium storage abilities in large capacity, high power, and long-life span.

In this article, we report an efficient method to synthesize $GeNb_{18}O_{47}$ nanowires (N-$GeNb_{18}O_{47}$) via a facile electrospinning way for the first time. As a control, the bulk $GeNb_{18}O_{47}$ (B-$GeNb_{18}O_{47}$) is formed through high temperature sol-gel method

* Corresponding author.
E-mail address: shujie@nbu.edu.cn (J. Shu).

https://doi.org/10.1016/j.electacta.2018.06.109
0013-4686/

reaction using the spinning precursor sol of $GeNb_{18}O_{47}$ nanowires. The structural, electrochemical characteristics and morphological of N-$GeNb_{18}O_{47}$ and B-$GeNb_{18}O_{47}$ are thoroughly investigated relying on many kinds of analytical methods. The results show that the different size of $GeNb_{18}O_{47}$ produced by different preparation methods has great influence on electrochemical properties.

2. Experimental section

2.1. Material preparation

The N-$GeNb_{18}O_{47}$ was synthesized by a facile electrospinning technique. According to the stoichiometric composition of $GeNb_{18}O_{47}$, $Ge(OCH_3)_4$ (Aladdin, 98%) and $Nb(OC_2H_5)_6$ (Aladdin, 99.9%) were dissolved in a specific solvent mixture as follows: 20 mL of ethanol solution and 1 mL of acetic acid solution. Next, 2.0 g of poly(vinylpyrrolidone) (PVP) was dissolved in the mixed solution to form the prepared precursor sol. After this, the spinning precursor sol was filled into a 10 mL syringe equipped with a 21-gauge stainless steel needle at a distance of 15 cm from the collector. 20 kV was the applied voltage between the needle and collector. Lastly, the obtained nanofibers were thermally treated at 950 °C for 15 h under an air atmosphere to acquire the final N-$GeNb_{18}O_{47}$. As a control, B-$GeNb_{18}O_{47}$ was fabricated through a facile sol-gel reaction method. First of all, we preheated the homogeneous $GeNb_{18}O_{47}$ precursor sol at 160 °C in the oven to form a dry gel, and then the dry gel was calcined at 1000 °C under the air atmosphere for 15 h to obtain B-$GeNb_{18}O_{47}$. Schematic diagram of the synthesis process for the N-$GeNb_{18}O_{47}$ and B-$GeNb_{18}O_{47}$ is shown in Fig. 1.

2.2. Sample characterization

The powder X-ray diffraction (XRD) patterns are determined by Bruker D8 Focus using Cu Ka radiation ($\lambda = 1.5406$ Å) in the 2θ angle from 10 to 50°. The size of the synthesized samples and surface morphologies were determined by using high-resolution transmission electron microscopy (HRTEM, JEOL JEM2010) and scanning electron microscopy (SEM, Hitachi SU-70) and.

2.3. Electrochemical measurement

The electrochemical performance test used a CR2032 coin-type cells, which consists of the lithium foil as counter electrode, a mixture of $LiPF_6$ in ethylene carbonate/dimethyl carbonate (1:1 by volume) as the electrolyte and the as-prepared material as working electrode. Here, the working electrodes were achieved by blending active materials (80 wt.%), polyvinylidene fluoride (10 wt.%) and carbon black (10 wt.%). All coin-type cells were fabricated in an argon-filled glovebox. The electrochemical behaviors were performed on a LANHE CT2001A battery test system. Moreover, cyclic voltammetry (CV) and electrochemical impedance spectra (EIS) were measured in a CHI660D electrochemical workstation. Here, the electrochemical observations were accomplished at 20 °C.

3. Results and discussion

Fig. 2 illustrates the XRD patterns of the resulting N-$GeNb_{18}O_{47}$ and B-$GeNb_{18}O_{47}$. According to the XRD pattern in Fig. 2a, there are several obvious diffraction peaks appearing at 17.87°, 23.97°, 25.35°, 26.56°, 31.15°, 33.22°, 36.15°, 46.74°, 37.04°, 38.84°, 43.87° and 47.59°, corresponding to the (310), (101), (420), (211), (321), (411), (620), (501), (521), (730) and (002) planes, respectively, of standard JCPDS card No.48-0888. It can be evidently found that there are no impurities peaks and no distinct differences in the XRD patterns of N-$GeNb_{18}O_{47}$ and B-$GeNb_{18}O_{47}$. In addition, the intensity and width of the N-$GeNb_{18}O_{47}$ peaks are clearly weaker and broader than those of the B-$GeNb_{18}O_{47}$ peaks. This phenomenon shows that the N-$GeNb_{18}O_{47}$ has a smaller grain size than B-$GeNb_{18}O_{47}$. From the Rietveld refinement results shown in Fig. 2b and c, it can be observed that the high pure $GeNb_{18}O_{47}$ samples are successfully prepared via both reactions, respectively.

The characterization results of microscopic morphology (SEM, TEM and mapping) for N-$GeNb_{18}O_{47}$ is shown in Fig. 3. We can observe that the SEM image of the electrospun precursor nanowires depicts an average diameter of ~200 nm nanofibers with smooth surfaces from Fig. 3a. After the high temperature calcination at 950 °C, their surfaces became even rougher and the average diameter of the compound N-$GeNb_{18}O_{47}$ was reduced to ~150 nm (Fig. 3b). Nevertheless, the morphology and diameter of B-$GeNb_{18}O_{47}$ compounded by a facile sol-gel method are completely different from those of N-$GeNb_{18}O_{47}$ owing to the effect of self-aggregation. It can be observed that the diameter of the B-$GeNb_{18}O_{47}$ was increased to 1–2 μm from the SEM images shown in Fig. 3c. As shown in Fig. 3d, we can see that the individual N-$GeNb_{18}O_{47}$ is composed of many nanoparticles. Fig. 3e and f shows the HRTEM images and the selected area electron diffraction (SAED) pattern of the N-$GeNb_{18}O_{47}$, indicating that detailed crystalline features are displayed. The interplanar distances are measured to be 0.3511 nm on the HRTEM images, matching very well with the (420) crystallographic plane of $GeNb_{18}O_{47}$. The SAED pattern is as well as the X-ray diffraction data in Fig. 2a, which both

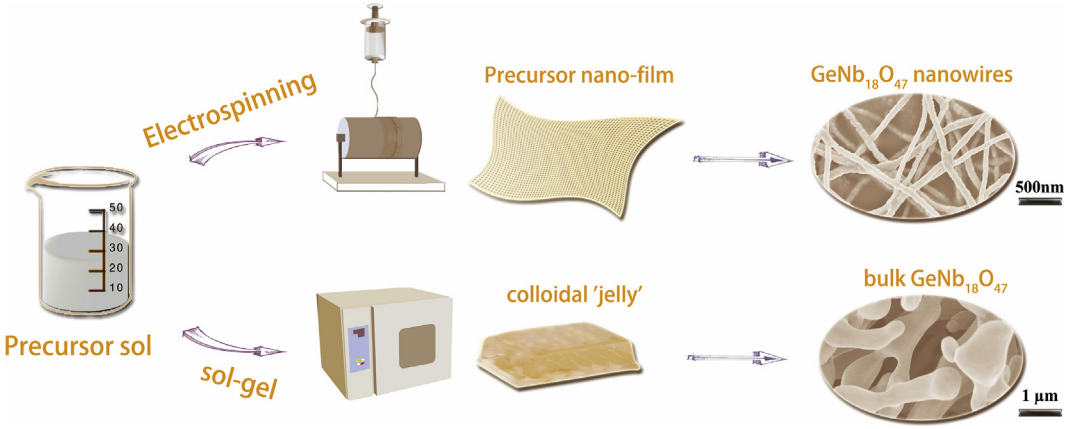

Fig. 1. Schematic illustration of the synthesis process for the N-$GeNb_{18}O_{47}$ and B-$GeNb_{18}O_{47}$.